Journal of Materials Chemistry C

Interface Disorder in Large Single- and Multi-Shell Upconverting Nanocrystals

Journal:	*Journal of Materials Chemistry C*
Manuscript ID	TC-ART-10-2018-005130.R1
Article Type:	Paper
Date Submitted by the Author:	23-Nov-2018
Complete List of Authors:	Hudry, Damien; Karlsruhe Institute of Technology, Institute of Microstructure Technology Popescu, Radian; Karlsruher Institut für Technologie, Laboratorium für Elektronenmikroskopie Busko, Dmitry; Karlsruhe Institute of Technology (KIT), Institute of Microstructure Technology Diaz-Lopez, Maria; Universit%e Grenoble Alpes, Institut Néel Abeykoon, Milinda; Brookhaven National Laboratory, Photon Science Division - National Synchrotron Light Source II Bordet, Pierre; Universite Grenoble Alpes, Institut Néel Gerthsen, Dagmar; Karlsruher Institut fur Technologie Howard, Ian; Karlsruher Institut fur Technologie, Institute of Microstructure Technology Richards, Bryce; Karlsruhe Institute of Technology (KIT), Institute of Microstructure Technology; Karlsruhe Institute of Technology (KIT), Light Technology Institute

Interface Disorder in Large Single- and Multi-Shell Upconverting Nanocrystals.

Damien Hudry,[1] Radian Popescu,[2] Dmitry Busko,[1] Maria Diaz-Lopez,[3] Milinda Abeykoon,[4] Pierre Bordet,[3] Dagmar Gerthsen,[2] Ian A. Howard,[1, 5] and Bryce S. Richards*[1,5]*

[1] Institute of Microstructure Technology, Karlsruhe Institute of Technology, Hermann-von-Helmholtz-Platz 1, D-76344 Eggenstein-Leopoldshafen, Germany.

[2] Laboratory of Electron Microscopy, Karlsruhe Institute of Technology, Engesserstrasse 7, D-76131 Karlsruhe, Germany.

[3] Université Grenoble Alpes, CNRS, Institut Néel, 38000 Grenoble, France.

[4] Photon Science Division, National Synchrotron Light Source II, Brookhaven National Laboratory, Upton, New York 11973, United States.

[5] Light Technology Institute, Karlsruhe Institute of Technology, Engesserstrasse 13, D-76131 Karlsruhe, Germany.

Abstract. The growth of core-shell nanocrystals (NCs) can lead to extended interface disorder due to the intermixing of core and shell materials. Such an issue is particularly important for large single- and multi-shell upconverting NCs, which have been considered as being relatively insusceptible to intermixing. In this work, a robust methodology – based on structure-independent local chemical analyses with nanometer-scale resolution and high-energy synchrotron x-ray powder diffraction – has been used to shed new light on the chemical and structural organization of large single-, double-, and triple-shell upconverting NCs. The experimental results reveal, for the first time, that significant disorder: i) exists at the interfaces of large (20 – 50 nm) multi-shell upconverting NCs; ii) reaches core-shell and shell-shell interfaces, independently of their position within the structure; iii) can be partially controlled by the shell deposition method; and iv) leads to the formation of multiple length-scale interfaces depending on the size of the starting seeds, the number and relative thickness of the pre-existing shells in the seeds. It is anticipated that the results will be beneficial in furthering the fundamental understanding of the structure–property relationships of multi-shell upconverting NCs.

Introduction. Over the last decade, numerous promising investigations on the practical utilization of lanthanide (Ln)-doped upconverting nanocrystals (NCs) have been reported, including their use in background-free biological sensing and light-triggered drug delivery,[1, 2] super resolution nanoscopy,[3] barcoding,[4] anti-counterfeiting,[5] and energy harvesting.[6] Two landmark developments significantly increased the performance of upconverting NCs; namely the introduction of the single-shell concept in 2004/2007,[7-10] followed by the multi-shell concept in 2011/2013.[11-14] The latter opened up tremendous possibilities to finely tune the upconversion (UC) properties of increasingly complex nanoscale upconverting architectures.[15-18]

The energy migration pathways that are used to control the optical properties of multi-shell upconverting NCs depend on the, yet unclear, chemical and structural order of core-shell and shell-shell interfaces. The precise description of multi-shell NCs in terms of crystal structure and chemical organization is particularly challenging due to the lack of chemical and crystallographic periodicity within individual NCs. Thus, the question as to how much disorder occurs at the interfaces of such NCs remains open. It has been considered that intermixing of core and shell materials is limited to ultra-small particles (<10 nm), which are more reactive than larger particles (>20 nm) and for which the intermixing effect is considered as being negligible or simply non-existent.[19] Thus, to date, large multi-shell upconverting NCs are considered as well-ordered systems with spatial separation of the optically active elements (i.e. Ln^{3+} cations) into nano-domains with abrupt interfaces, as schematically illustrated in Figure 1A. However, preliminary investigations performed on single-shell structures suggested that the chemical organization of multi-shell NCs could be subtler and more complicated leading, in certain cases, to extended intermixing (Figure 1B). The idea was first postulated by van Veggel *et al.*[20] nearly a decade ago for single-shell NCs. Spectroscopic evidence in favor of van Veggel's assumption was provided six years later by Haase and co-workers via the energy transfer between 2-naphthoic acid – located at the surface of the NCs – and Eu^{3+} in $NaEuF_4/NaGdF_4$ (14.4 nm $\pm$ 5.5 %).[21]

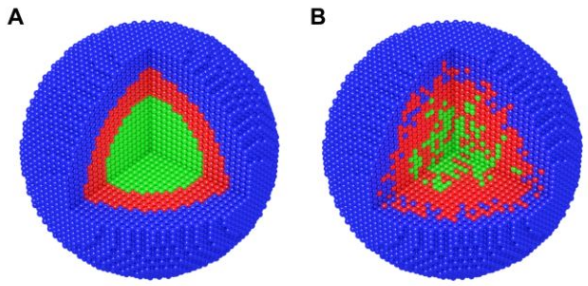

Figure 1. *Schematic representations of double-shell (C2S) upconverting nanocrystals showing the 'sharp interfaces' (A) and 'intermixed' (B) models. In A, chemically and structurally well-defined homogeneous nano-domains are characterized by abrupt interfaces. On the other hand, in B, the shell growth leads to chemically and structurally non-homogeneous nano-domains characterized by diffuse interfaces on different length-scales and, thus, chemical and structural disorder.*

In 2017, Hudry *et al.* performed structure-independent local chemical analyses with nanometer-scale resolution on ultra-small $NaGdF_4$:Yb:Er / $NaYF_4$ single-shell NCs (starting seeds: 4.8 ± 0.5 nm).[22] This yielded, for the first time, detailed chemical maps of single-shell structures with various shell thicknesses and revealed the existence of diffuse interfaces characterized by chemical concentration gradients. This was in contrast to earlier work by Chen *et al.,* who reported that the structural integrity of ultra-thin (3 nm) $NaYF_4$:Tb shells deposited on very large (40 nm) $NaYF_4$:Ce core NCs was retained.[19] It is important to note that the intermixing effect observed for upconverting NCs is in alignment with earlier research on core quantum dots (QDs). For example, Alivisatos *et al.*[23] discovered that QDs are chemically dynamic systems and are, thus, more prone to mixing than their bulk counterparts. A recent review by Chang *et al.*[24] on interfacial engineering of single- and multi-shell QDs clearly shows that spectroscopic analyses combined with structural characterization can unveil the important role played by interfaces in controlling optical properties of QDs. Finally, cation exchange reactions with preformed NCs trigger various multi-parameter dependent (temperature, association and dissociation energies, solvation and desolvation energies, nature of coordinating ligands in the growth media, and miscibility of the different phases) transformations within the final architecture as recently reviewed by De Trizio and Manna.[25]

To date, the magnitude of the intermixing effect in large single- and multi-shell upconverting NCs remains unknown, despite such NCs representing >90% of the structures reported in the literature, including the most recent developments.[26, 27] Moreover, three main shell deposition methods are classically used and reported in the literature to synthesize single- and multi-shell upconverting NCs,[28-30] but the influence of such methods on the final chemical

and structural organizations of the as-prepared core-shell structures is also unknown. Finally, large multi-shell upconverting NCs are of major interest because they can bridge the existing gap between extreme cases that were recently reported.[19, 21, 22] Thus, it is very likely that interface formation in large single- and multi-shell upconverting NCs is a multi-parameter dependent effect whose magnitude in terms of interface thickness as well as chemical or structural disorder can be controlled.

Herein, we use structure-independent local energy dispersive x-ray spectroscopy (EDXS) in a transmission electron microscope (TEM) and high-energy synchrotron x-ray powder diffraction (XPD) to demonstrate that the intermixing of core-shell and shell-shell layers occurs during the synthesis of large single- (CS), double- (C2S) and triple- (C3S) shell upconverting NCs up to 50 nm. Despite the relatively large size (~20 nm) of the starting seeds, the investigated multi-shell NCs exhibit the formation of diffuse and inhomogeneous interfaces on multiple length-scales. Unexpectedly, the deposition of the first shell ($NaYF_4$) did not protect the integrity of the core during the deposition of the second shell ($NaGdF_4$). The latter is once again modified when adding the third shell ($NaYF_4$). Additionally, intermixing was observed for the three main shell deposition methods,[28-30] which are classically used for the growth of single- and multi-shell upconverting NCs. Interestingly, differences regarding the magnitude of the intermixing effect were observed depending on the shell deposition method that was used. Our findings constitute a novel evidence in favor of complex interfaces in large single- and multi-shell upconverting NCs in a size-range covered by >90% of the UC nanoparticle literature. The results presented constitute an important step towards properly describing the organization of such complex functional nanomaterials, which have to be considered as non-periodic modulated structures.

Large single-shell upconverting NCs. Three main synthetic methods are classically used and reported in the literature to synthesize high quality single-shell (CS) upconverting NCs.[28-30] Differences between the synthetic methods are mainly related to the chemical nature of the starting rare-earth, sodium, and fluorine precursors, as well as the way shell precursors are injected into the seeds solution. With time, all three synthetic methods have been refined but their basic principles have not changed. The first synthetic method (Method I) that was reported to synthesize CS upconverting NCs is based on the controlled hot-injection at high temperature of the shell precursor solution into a hot solution containing the starting core NCs. Such a method is characterized by the utilization of sodium trifluoroacetate ($NaOOCCF_3$) as a single-source precursor for sodium and fluorine. The single-source precursor is used in combination with rare-earth trifluoroacetates.[28] The second synthetic method (Method II) was first reported in 2008 and is based on the utilization of sodium hydroxide (NaOH) and ammonium fluoride (NH_4F) as dual-source precursors for sodium and fluorine in combination with rare-earth chlorides or acetates.[29] The starting core NCs are directly added into the shell solution at low temperature (50-80°C) and the resulting mixture is heated up to the target temperature (usually 280-310°C). Note that as for the synthetic Method I, the shell precursor solution can also be injected at high temperature. Finally, the most recent synthetic method (Method III) was first reported in 2012.[30] Contrary to Methods I and II, small α-$NaLnF_4$ (cubic phase) NCs are used as shell precursors (also known as sacrificial seeds) and injected at high temperature into a hot solution containing the starting seeds. Such a modification of the chemistry can not only modify shell growth mechanisms, but also the chemical stability of the initial seeds within the growth medium. All three synthetic methods have been used in this study to first prepare CS upconverting NCs. To enable a fair comparison between the different methods (Methods I, II, and III), all shell growth experiments were performed by using the exact same isotropic $NaEr_{0.8}Yb_{0.2}F_4$ core (C) NCs. (average diameter: 21 $\pm$ 2 nm; Figure S1) as the starting seeds to grow $NaEr_{0.8}Yb_{0.2}F_4$ / $NaYF_4$ CS_x structures (with x = I, II, or III - referring to the synthetic method used).

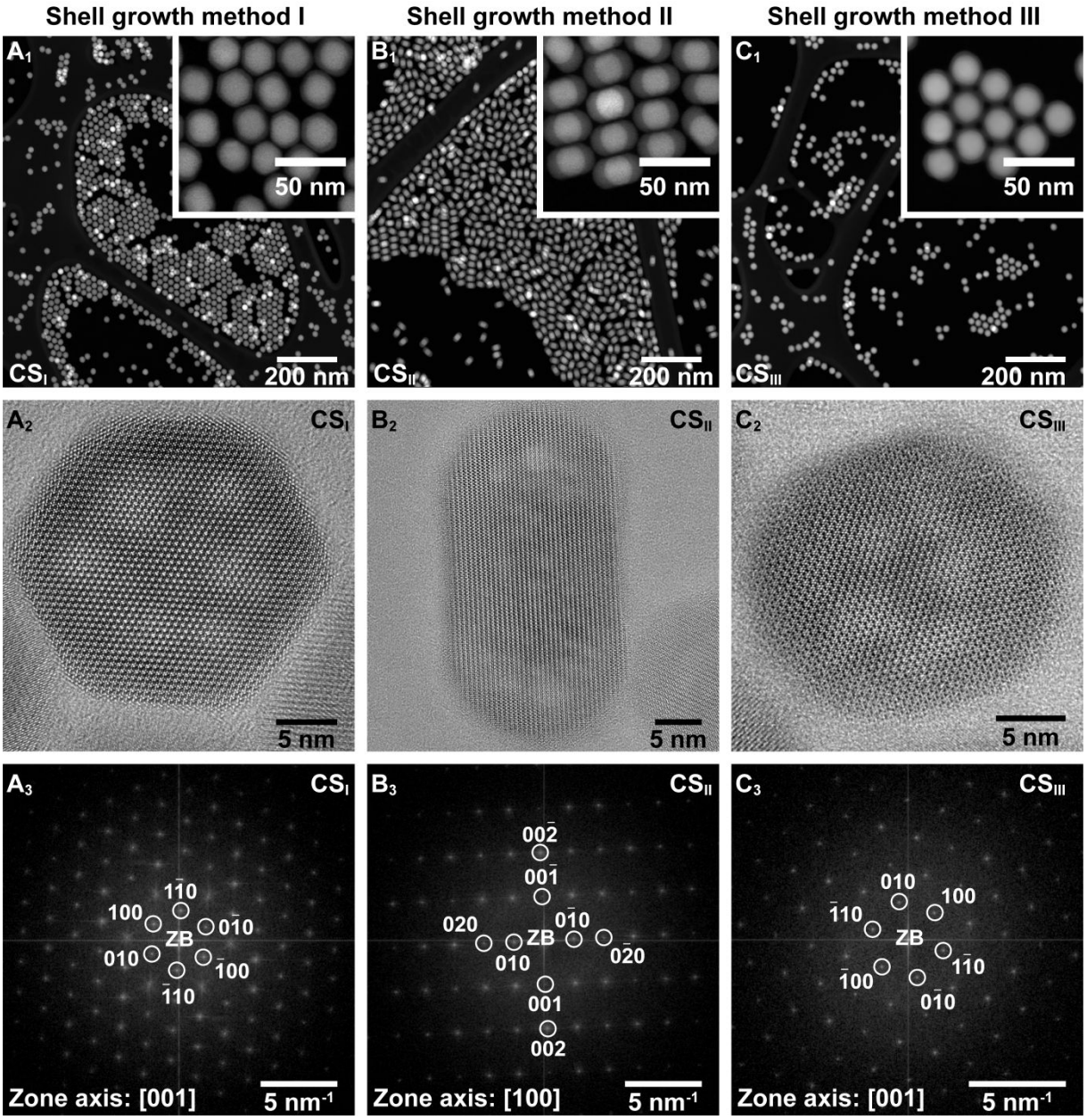

Figure 2. *(A_1-C_1) High-angle annular dark-field scanning transmission electron microscopy (HAADF-STEM) micrographs, (A_2-C_2) high-resolution transmission electron microscopy micrographs with (A_3-C_3) their corresponding two-dimensional Fourier-transform (FT) patterns of $NaEr_{0.8}Yb_{0.2}F_4$ / $NaYF_4$ CS upconverting nanocrystals (NCs). The latter where synthesized by the three main shell deposition methods typically used by research groups worldwide (method I – left column; method II – middle column; and method III – right column). The indexing of the two-dimensional FT patterns is compatible with the formation of the hexagonal phase (β-phase, space group $P\bar{6}$, # 174). Insets in panels A_1-C_1 show magnified areas. The exact same core NCs were used as the starting seeds for the synthesis of the CS_I, CS_{II}, and CS_{III} NCs.*

Additionally, the exact same growth conditions (concentration, controlled hot-injection, temperature, time, injection rate) were used for the three different methods with the exception of the shell precursors. Detailed experimental information is given in the Supporting Information (SI). The as-prepared CS_I, CS_{II}, and CS_{III} NCs have been characterized by scanning TEM (STEM) (Figure 2 A_1-C_1), and high-resolution (HR) TEM (Figure 2 A_2-C_2) combined with two-dimensional Fourier transform patterns (Figure 2 A_3-C_3).

Such classical characterizations revealed qualitative information such as: i) the formation of highly monodisperse isotropic CS NCs independently of the shell deposition method; ii) heterogeneities in terms of chemical composition within single CS NCs compared to the pure C NCs; and iii) the formation of apparently single crystalline phases for all synthesized CS NCs. Note that although the exact same seeds and shell growth conditions (with the exception of the shell precursors) have been used for the synthesis of the different CS structures, the shape of the latter can be modified. Indeed, whereas both CS_I and CS_{III} NCs are isotropic, CS_{II} NCs are highly anisotropic with the formation of nanorods. This clearly indicates that intermediate species or shell precursors, can dramatically modify the output of the synthesis. From HRTEM micrographs (Figure 2 A_2-C_2) and their corresponding two-dimensional FT patterns (Figure 2 A_3-C_3), it is obvious that all NCs are highly crystalline and individual particles can be apparently described as single crystalline domains. The indexation of the corresponding FT patterns is in perfect agreement with the formation of the hexagonal phase (space group $P\bar{6}$, #174) with no indication of secondary phase such as the cubic phase (space group $Fm\bar{3}m$, #225). It is worth noting that HRTEM has some limitations when dealing with the characterization of single-shell upconverting NCs because i) the resolution is not sufficient to distinguish the formation of isostructural phases with very similar cell parameters, and ii) the discrimination between epitaxial growth on one hand and the reorganization of the structure as a consequence of the formation of a solid-solution (due for example to intermixing) on the other hand, is not possible especially without modeling. Note that such limitations also apply to classical x-ray powder diffraction (XPD). Finally, the elemental maps of CS_I, CS_{II}, and CS_{III} NCs (Figure 3) obtained by classical EDXS show, as expected, the formation of single-shell structures and the heterogeneous distribution of the core (erbium / ytterbium) and shell (yttrium) elements. Nevertheless, it is important to note that the local distributions of the different core and shell elements within individual CS NCs cannot be extracted from the presented chemical maps due to the two-dimensional projection of three-dimensional objects.

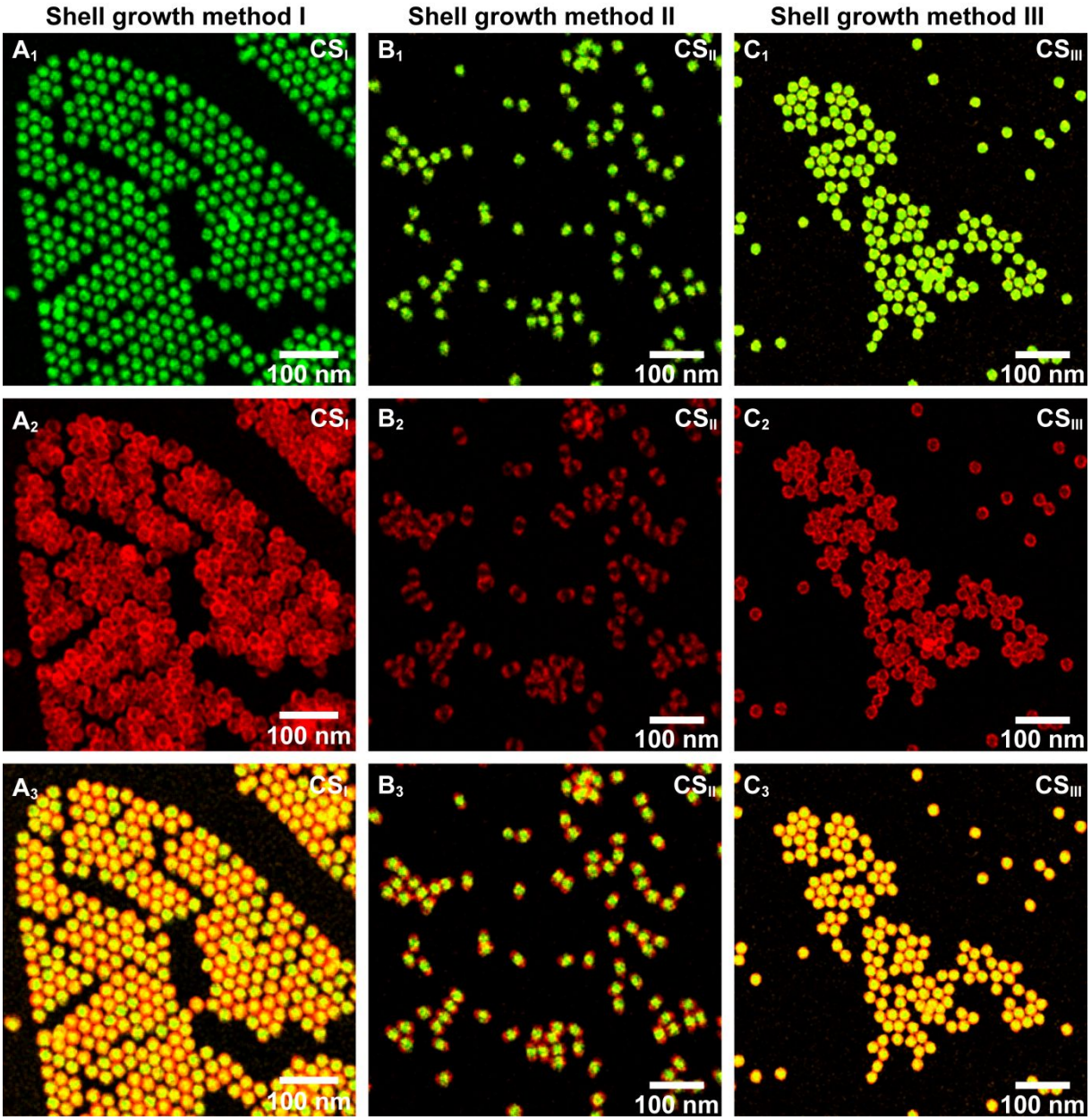

Figure 3. *Elemental maps obtained by energy dispersive x-ray spectroscopy (EDXS) of $NaEr_{0.8}Yb_{0.2}F_4$ / $NaYF_4$ CS upconverting nanocrystals (NCs) synthesized by the three main shell deposition methods typically used by research groups worldwide (method I – left column; method II – middle column; and method III – right column). (A_1-C_1) erbium / ytterbium maps, (A_2-C_2) yttrium maps, and (A_3-C_3) combined erbium / ytterbium, and yttrium maps. The exact same core NCs were used as the starting seeds for the synthesis of the CS_I, CS_{II}, and CS_{III} NCs.*

As a consequence, reliable information relative to the chemical and structural organization – such as ordered vs. disordered, chemical gradients, cell parameters, strain – of the as-prepared CS NCs cannot be extracted from direct observations relative to classical characterization techniques and can lead to misleading interpretations.

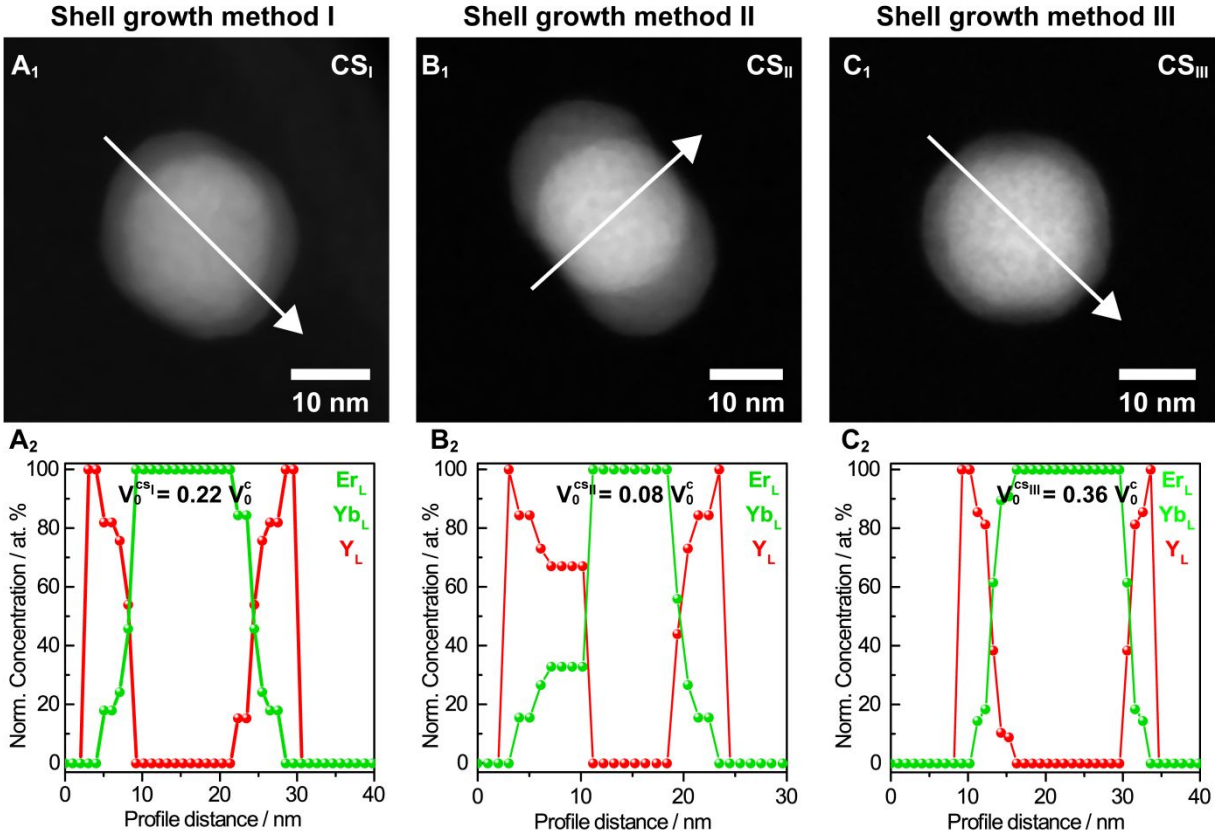

Figure 4. *(A_1-C_1) High-angle annular dark-field scanning transmission electron microscopy (HAADF-STEM) micrographs with white arrows indicating the energy dispersive x-ray spectroscopy (EDXS) scan directions of individual $NaEr_{0.8}Yb_{0.2}F_4$ / $NaYF_4$ CS upconverting nanocrystals (NCs), and (A_2-C_2) their corresponding structure-independent concentration profiles (erbium/ytterbium – green; yttrium – red). Upconverting NCs were synthesized by three different shell deposition methods (method I – left column; method II – middle column; and method III – right column). The volumetric fractions of the pure core (V_0) regions (i.e. erbium / ytterbium) in CS_I ($V_0^{CS_I}$), CS_{II} ($V_0^{CS_{II}}$), and CS_{III} ($V_0^{CS_{III}}$) NCs relative to the initial average volume of the starting core NCs (V_0^C) are indicated. The exact same core NCs were used as the starting seeds for the synthesis of the CS_I, CS_{II}, and CS_{III} NCs.*

In 2017, our group took advantage of a new methodology to extract local chemical information in ultra-small single-shell upconverting NCs (< 10 nm) from line scan EDXS analyses performed on individual particles. The method, first developed by Kind *et al.*,[31] enables to take into account (for each measuring point) the local contribution of the surrounding environment leading to a structure-independent chemical profile with nanometer-scale resolution. Interestingly, the methodology can be applied independently of the number of shells that are grown because of the sub-shell division model combined to the iterative data processing treatment (Supporting Information). The as-prepared CS_I, CS_{II}, and CS_{III} NCs that were characterized by this technique are presented in Figure 4 (A_1-C_1). Contrast variation within individual particles can be observed for CS_I (Figure 4A_1), CS_{II} (Figure 4B_1) and CS_{III} (Figure 4C_1) NCs. Note that such a contrast is absent in the pure C NCs (Figure S2). The corresponding structure-independent chemical profiles in Figure 4 (A_2-C_2) were

extracted from line scans (Figures $4A_1$-C_1, white arrows) after normalization relative to the total quantity of Ln^{3+} (Figure S3). Sodium and fluorine were removed for clarity because no disorder is expected for those elements (both of them are host elements for core and shell materials). For all CS NCs, erbium and ytterbium signals were simultaneously integrated and treated as a single entity (ΣEr,Yb). Typical results obtained for shell deposition methods I (Figure 4A), II (Figure 4B), and III (Figure 4C) clearly indicate that the corresponding chemical organization of the final CS structure is modified depending on the shell deposition method (although the starting seeds were identical). The shape parameter aside, the volumetric fraction (relative to the average volume V_0^c of the pure core NC acting as seed) of the pure core region in the final CS NCs ($V_0^{CS_I}$, $V_0^{CS_{II}}$, $V_0^{CS_{III}}$) decreases down to 8% for the shell deposition method II, whereas it is 4.5 times larger (36%) for the shell deposition method III. Note that the shell deposition method I is intermediate with a volumetric fraction of 22%. The pure core region (erbium/ytterbium) of CS_I, CS_{II}, and CS_{III} NCs is surrounded by an inhomogeneous and relatively thick shell whose chemical composition regularly changes from an (erbium / ytterbium)-rich solid-solution to an Y-rich one within 4 to 6 nm from the surface of the pure core region. The non-homogeneous interface region is surrounded by a thin (1-2 nm) homogeneous shell of pure yttrium. Note that in the case of anisotropic nanorods (CS_{II} sample), the longitudinal chemical analysis (Figure S4) clearly reveals the formation of a thicker Y-based shell along the long axis. The analyses clearly show that not only optically active elements (erbium / ytterbium) are partially diluted during the growth of the yttrium-based shell, but also that there is a non-zero probability to find such optically active elements close to the surface. Although the degree of intermixing is less pronounced compared to ultra-small CS NCs, it is still significant and the volume of the interface (within which chemical concentration gradients appear) can represent as much as 70 % of the total CS volume. This constitutes the first experimental evidence that the three shell deposition methods universally used by the UC community are dramatically different regarding the magnitude of the intermixing effect independently of the size of the starting seeds.

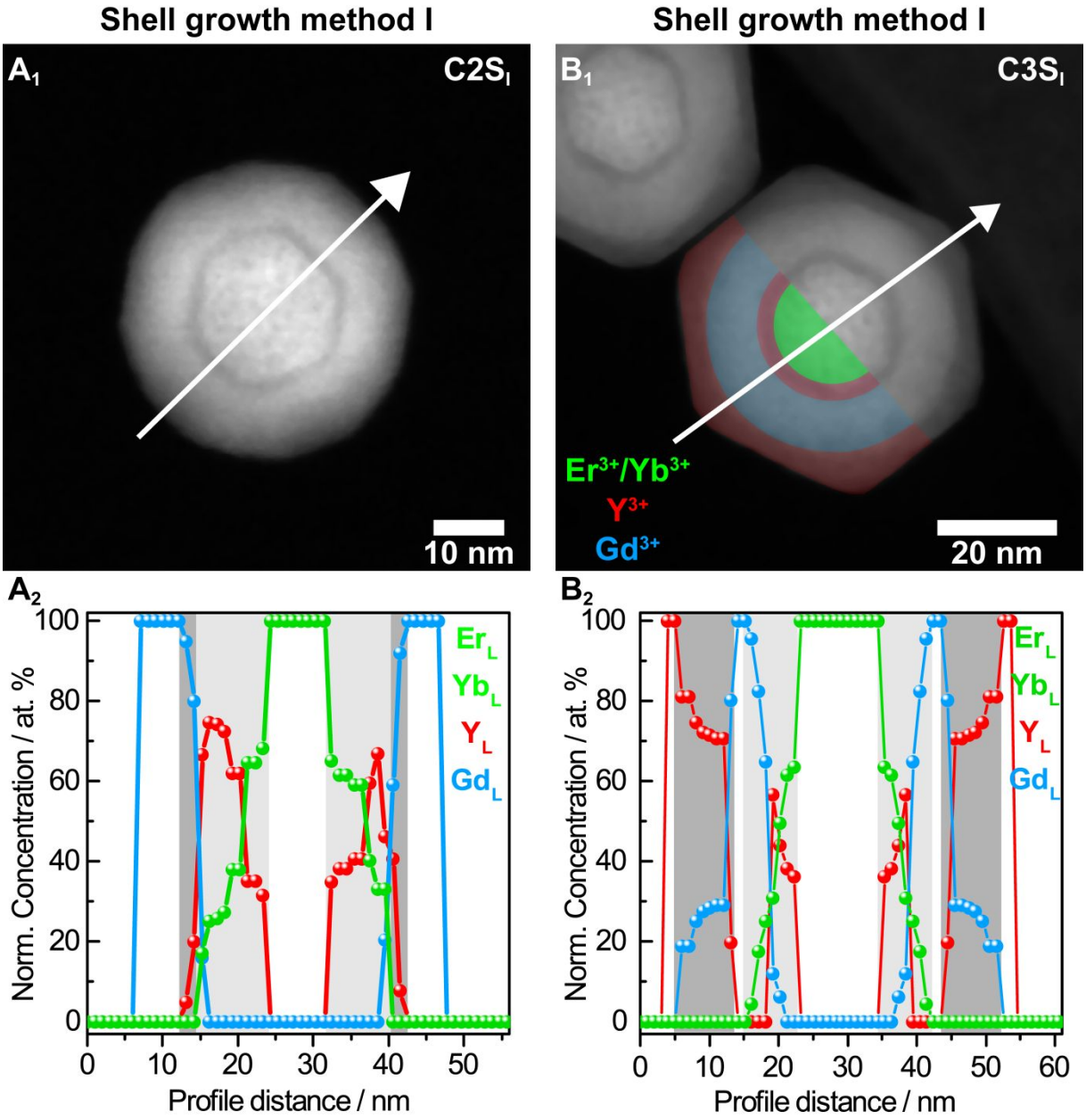

Figure 5. *(A_1-B_1) High-angle annular dark-field scanning transmission electron microscopy (HAADF-STEM) micrographs with white arrows indicating the energy dispersive x-ray spectroscopy (EDXS) scan directions of individual $NaEr_{0.8}Yb_{0.2}F_4$ / $NaYF_4$ / $NaGdF_4$ double-shell C2S, and $NaEr_{0.8}Yb_{0.2}F_4$ / $NaYF_4$ / $NaGdF_4$ / $NaYF_4$ triple-shell C3S nanocrystals synthesized by the shell deposition method I. (A_2-B_2) Corresponding structure-independent concentration profiles (erbium/ytterbium – green; yttrium – red; and gadolinium – blue). The exact same core NCs were used as the starting seeds for the synthesis of the $C2S_I$, and $C3S_I$ NCs. Colorized overlaid layers on the HAADF-STEM micrograph (B1) show the classical interpretation for the distribution of lanthanide ions when only relying on a contrast-based analysis.*

Large multi-shell upconverting NCs. The size of the NCs used as starting seeds to grow multi-shell structures is not always the most relevant parameter to be considered when dealing with intermixing. Indeed, the number of pre-existing shells together with their relative thickness can be just as important. Thus, $NaEr_{0.8}Yb_{0.2}F_4/NaYF_4/NaGdF_4$ C2S and $NaEr_{0.8}Yb_{0.2}F_4/NaYF_4/NaGdF_4/NaYF_4$ C3S NCs were synthesized (Figure 5 and Figures S5-

S6) by the shell deposition method I to probe the modification of the chemical organization when growing multi-shell structures. For the double-shell structure, after the growth of the second gadolinium-based shell (Figure 5 A_1-A_2), the size of the $C2S_I$ NC increases up to 42 nm (average diameter 42 $\pm$ 6 nm). Interestingly and despite the growth of the primary yttrium-based shell (CS_I), the whole chemical composition is once again modified. The size of the pure erbium / ytterbium C (Figure 5A_2) shrinks to 8 nm (average 7 $\pm$ 2 nm measured on four particles). A thick (7.5 – 9 nm) (erbium-ytterbium) / yttrium interface is formed with two different regions. The closest to the pure erbium-ytterbium core region is composed of 60 % erbium-ytterbium and 40 % yttrium whereas the farthest is composed of 35 % erbium-ytterbium and 65 % yttrium. Interestingly, the thin (2 nm) pure yttrium-based shell that characterized the outer region of the CS_I seeds has completely disappeared and is replaced by a second interface of 2.5 nm, which is mainly composed of yttrium and gadolinium into various proportions. Note that the inner region of this second interface is characterized by the presence of all elements (erbium-ytterbium, yttrium, and gadolinium) in an ultra-thin (ca. 1 nm) layer. The second interface is surrounded by a thick (5 – 6 nm) and pure gadolinium shell. It is worth noting that for the final C2S architecture, the pure C region represents only 1 % of the total volume of the NC whereas the combined volume of all interfaces and the volume of the pure outer shell represent 34 % and 65 %, respectively.

Similarly, $C3S_I$ NCs were synthesized. Note in that case the amount of injected shell precursors was decreased (compared to the synthesis of $CS2_I$ NCs) to limit the final size of the NCs (see details in the supporting information). As shown in Figure 5 (B_1-B_2), intermixing is still significant in a C3S structure. Colorized overlaid layers on the HAADF-STEM micrograph (Figure 5B_1) illustrate the distribution of the different Ln^{3+} elements within the particle. The chemical organization is typically derived from a direct contrast-based analysis of the HAADF-STEM micrograph. The clear limits between the dark (attributed to yttrium) and bright (attributed to be erbium-ytterbium or gadolinium) regions on the HAADF-STEM micrograph (no processing treatment have been used to either modify or improve the

contrast) are sometimes considered as evidence of the formation of a large multi-shell structure with sharp interfaces. However, the structure-independent chemical profiles presented in Figure $5B_2$ reveal a different story as to that conveyed by the contrast-based analysis of the corresponding HAADF-STEM micrograph (Figure 5A). Although the particle analyzed is large (51 nm), chemically pure interfaces are either non-existent or ultra-thin (1 nm at best). More importantly, chemical elements supposed to be confined in the core region are in reality in direct contact with chemical elements from the first and second shells within a relatively thick interface of ca. 8 nm (light gray regions, Figure $5B_2$) with concentration gradients. Similarly, chemical elements from the second and third shells are in direct contact within a diffuse interface of ca. 10 nm (dark gray regions, Figure $5B_2$).

Investigations performed on large double- and triple-shell structures constitute for the first time direct evidence that extended disorder reaches all chemical domains (initially designed to be independent) of a multi-shell architecture despite the relatively large size of the final structure (50 nm), which is at the upper limit of the size regime usually reported in the literature for such architectures.

Structural Characterization. High-energy synchrotron XPD data of C_l, CS_l and $C2S_l$ NCs were indexed to hexagonal β-$NaLnF_4$ with space group $P\overline{6}$,[32] with the absence of extra peaks that could be assigned to crystalline impurity phases. These data were examined in reciprocal space via Rietveld refinement of background removed patterns, and in real space by the fitting of the pair distribution function (PDF) at short (1.5-15 Å) and long (15-30 Å) interatomic (r)-ranges. For all three samples, excellent fits to the experimental data with reasonable refined parameters were produced (Figure 6) with a one-phase model for both C_l and CS_l NCs and a two-phase model for $C2S_l$ NCs. The good agreement obtained between reciprocal and real space refined parameters (Tables S1-S2), further supports the veracity of these results. XPD data are in agreement with the models derived from local elemental EDXS analyses.

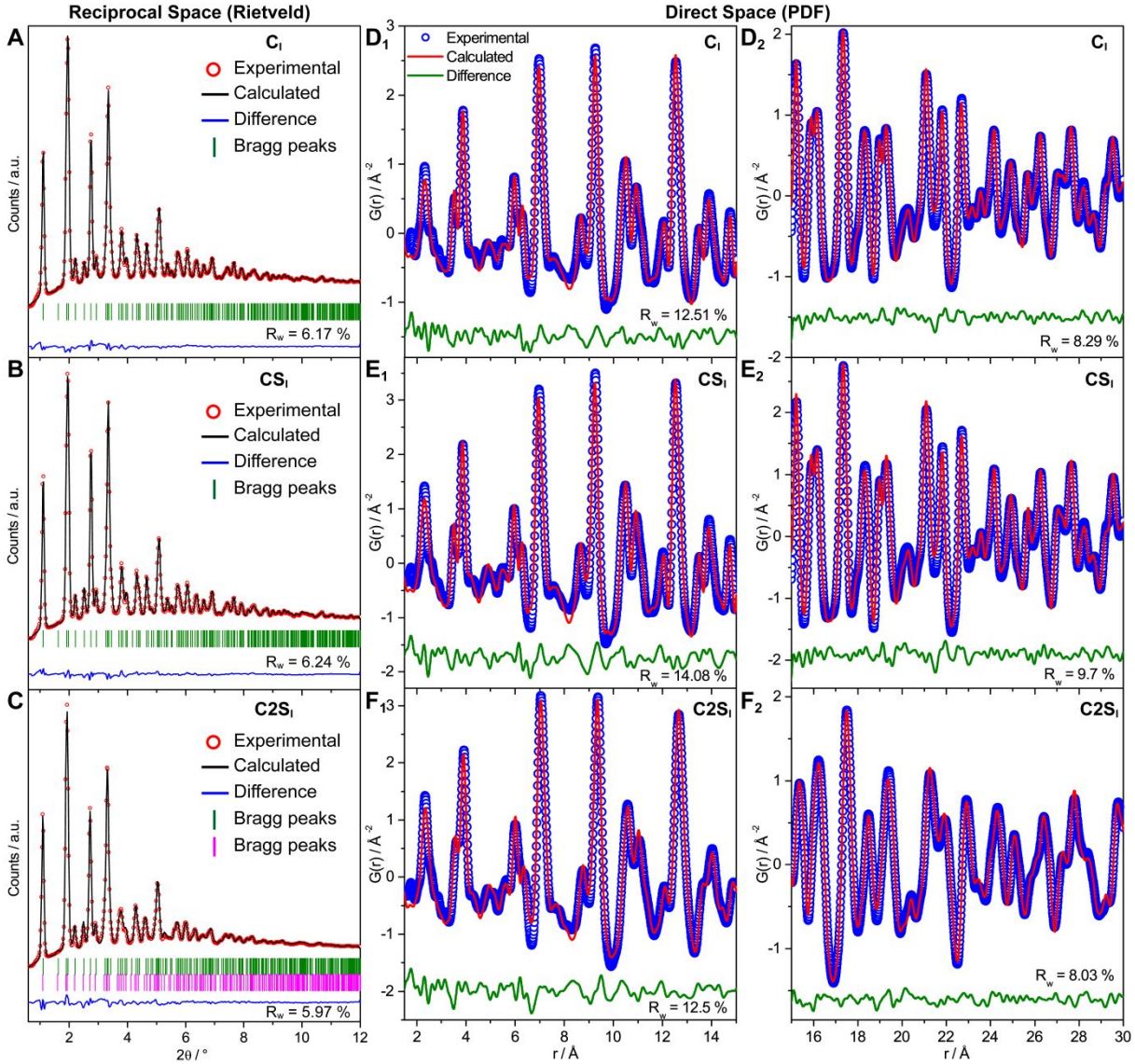

Figure 6. *(A-C) Rietveld refinements of $NaEr_{0.8}Yb_{0.2}F_4$ C_l (A), $NaEr_{0.8}Yb_{0.2}F_4$ / NaYF4 CS_l (B), and $NaEr_{0.8}Yb_{0.2}F_4$ / $NaYF_4$ / $NaGdF_4$ $C2S_l$ (C) nanocrystals (NCs). Red circles and black lines represent the experimental and calculated XPD patterns, respectively. The blue lines (shifted for clarity) show the difference between experimental and calculated XPD patterns. Bragg peaks positions are indicated by green (phase 1) and magenta (phase 2) tick marks. For all refinements the goodness of fit (R_W value) is indicated (bottom right). (D-F) PDF refinements of $NaEr_{0.8}Yb_{0.2}F_4$ C_l ($D_{1\text{-}2}$), $NaEr_{0.8}Yb_{0.2}F_4$ / $NaYF_4$ CS_l ($E_{1\text{-}2}$), and $NaEr_{0.8}Yb_{0.2}F_4$ / $NaYF_4$ / $NaGdF_4$ $C2S_l$ ($F_{1\text{-}2}$) upconverting NCs. Blue circles and red lines represent the experimental and calculated PDFs, respectively. The green lines (shifted for clarity) show the difference between experimental and calculated PDFs. Refinements were performed with a one-phase model (D, E) and a two-phase model (F). PDF refinements were performed for the short- (middle column) and long r-ranges (right column). For all refinements the goodness of fit (R_W value) is indicated (bottom right).*

The refinements were carried out as a one-phase model for C_l and CS_l NCs with chemical compositions $NaEr_{0.8}Yb_{0.2}F_4$ and $Na(\sum Er,Yb)_{0.5}Y_{0.5}F_4$, respectively (obtained from Figure $4A_2$). The mean particles' diameters determined by HAADF-STEM are in good agreement with the size of the coherent domains refined by Rietveld (16 nm and 24 nm for C_l and CS_l NCs, respectively) and within the errors for the PDF-refined values with larger uncertainties. The matching of particles' diameters with the sizes of the coherent domains is an indication of well-defined internal order of dispersed NCs. No significant changes in the lattice

parameters, sample strain or segregation of phases could be identified when coating the $NaEr_{0.8}Yb_{0.2}F_4$ C_l with a thin shell of $NaYF_4$ (CS_l), due to the similar ionic radii of Y^{3+} with only ~1 % of mismatch with respect to those of Er^{3+} and Yb^{3+}.[33] In a first approximation, the CS_l NCs can be described as a solid-solution in agreement with the results obtained for ultra-small single-shell NCs.[22]

However, when a second gadolinium-based shell (with a larger ionic radii mismatch of ~5 %)[33] is deposited onto the CS_l structure ($C2S_l$), both a shift in the position and broadening of the XPD and PDF peaks is observed. In this case the reciprocal (Figure S7) and real (Figure S8) space refinements were significantly improved when adding an extra phase ($P\bar{6}$) in the refinements of $C2S_l$ (Figures 6C and $6F_{1\text{-}2}$). The compositions of the two phases included in the refinement of $C2S_l$ were fixed to match $Na(\sum Er,Yb)_{0.5}Y_{0.5}F_4$ for the inner part (Phase 1) and $NaGdF_4$ for the outer part (Phase 2) with larger lattice parameters. Note that the refined volume fractions for these two phases (Table S2) are in good agreement with the volumes previously estimated by HAADF-STEM. When comparing these results with the ones previously published for ultra-small single-shell NCs,[22] it clearly appears that the degree of disorder is modified as a function of the size of the starting seeds and the relative shell thickness. Note that the emission properties of the as-prepared C, CS, and C2S NCs can be used as complementary spectroscopic tools to probe chemical disorder (Figures S9-S11).

Single- and multi-shell NCs are challenging materials because their atomic-scale structures cannot be easily revealed. Indeed, such complex nanomaterials are non-periodic by nature and chemically modulated on multiple length-scales as revealed by structure-independent local chemical analyses. As a consequence, it is no longer possible to identify and define a single unit cell that is representative of the whole structure (neither in terms of chemistry or cell parameters). This constitutes a major challenge in either the reciprocal or real space Rietveld refinements where compositional gradients are dealt with as average compositions. Nevertheless, it is still possible to extract qualitative and valuable information. Indeed, analysis of peaks shifting and peaks broadening after each shell deposition gives a good

indication regarding the degree of intermixing, and thus disorder within NCs. Solving the atomic-scale structure of single- and multi-shell upconverting NCs requires the development of dedicated tools combined in a complex modeling framework, which is currently under development.

Conclusion. Compared to ultra-small (< 10 nm) upconverting NCs with large surface energy, large upconverting NCs (> 20 nm) are more stable, and thus, have been considered as being relatively insusceptible to intermixing effect. This motivated the present manuscript, which relies on novel evidence to provide new insights to the real nature and magnitude of disorder in large single- and multi-shell upconverting NCs. The experimental evidence revealed, for the first time, that: i) significant disorder exists at the interfaces of multi-shell NCs up to 50 nm; ii) disorder reaches all interfaces independently of their position within the architecture; iii) such disorder can be modified to a certain extent by the shell deposition method; and iv) disorder is characterized by the formation of chemically non-homogeneous and diffuse interfaces on multiple length-scales depending on the size of the starting seeds and also on the number and relative thickness of the pre-existing shells in the seeds. Although the degree of disorder varies somewhat, it is not clear yet whether, and under which conditions, intermixing can be suppressed. This new set of evidence combined with those previously obtained with ultra-small (<10 nm)[22] and small (<20 nm)[21] single-shell upconverting NCs clearly indicate that both single- and multi-shell upconverting NCs have to be described as non-periodic modulated structures. Note that typical examples reported in this contribution cover the vast majority of core-shell upconverting structures reported in the literature up to now. At the time where controlling multi-shell upconverting NCs (including sub-10 nm architectures) with atomic precision is highly desired,[34] our results constitute an important step towards the comprehensive understanding of the structure-property relationships of such technologically important luminescent nanomaterials.

Acknowledgement

D.H. would like to thank Marion Lenzner for TG analyses. The authors would also like to acknowledge the financial support provided by Helmholtz Recruitment Initiative Fellowship (B.S.R.) and the Helmholtz Association's research program Science and Technology of Nanosystems (STN). The authors would like to thank the Karlsruhe Nano Micro Facility (KNMF) for TEM access. This research used resources of the National Synchrotron Light Source II (beamline 28-ID), a U.S. Department of Energy (DOE) Office of Science User Facility operated for the DOE Office of Science by Brookhaven National Laboratory under Contract No. DE-SC0012704.

References

1. L. Zhou, R. Wang, C. Yao, X. Li, C. Wang, X. Zhang, C. Xu, A. Zeng, D. Zhao and F. Zhang, *Nature Communications*, 2015, **6**, 6938.
2. L. Zhou, Z. Chen, K. Dong, M. Yin, J. Ren and X. Qu, *Adv. Mater.*, 2014, **26**, 2424-2430.
3. Y. Liu, Y. Lu, X. Yang, X. Zheng, S. Wen, F. Wang, X. Vidal, J. Zhao, D. Liu, Z. Zhou, C. Ma, J. Zhou, J. A. Piper, P. Xi and D. Jin, *Nature*, 2017, **543**, 229-233.
4. J. Lee, P. W. Bisso, R. L. Srinivas, J. J. Kim, A. J. Swiston and P. S. Doyle, *Nat Mater*, 2014, **13**, 524-529.
5. M. You, J. Zhong, Y. Hong, Z. Duan, M. Lin and F. Xu, *Nanoscale*, 2015, **7**, 4423-4431.
6. W. Shao, G. Chen, T. Y. Ohulchanskyy, C. Yang, H. Agren and P. N. Prasad, *Nanoscale*, 2017, **9**, 1934-1941.
7. O. Lehmann, K. Kömpe and M. Haase, *J. Am. Chem. Soc.*, 2004, **126**, 14935-14942.
8. H.-X. Mai, Y.-W. Zhang, L.-D. Sun and C.-H. Yan, *J. Phys. Chem. C*, 2007, **111**, 13721-13729.
9. J.-C. Boyer, J. Gagnon, L. A. Cuccia and J. A. Capobianco, *Chem. Mater.*, 2007, **19**, 3358-3360.
10. H. Schäfer, P. Ptacek, O. Zerzouf and M. Haase, *Adv. Funct. Mater.*, 2008, **18**, 2913-2918.
11. Q. Su, S. Han, X. Xie, H. Zhu, H. Chen, C.-K. Chen, R.-S. Liu, X. Chen, F. Wang and X. Liu, *J. Am. Chem. Soc.*, 2012, **134**, 20849-20857.
12. F. Wang, R. Deng, J. Wang, Q. Wang, Y. Han, H. Zhu, X. Chen and X. Liu, *Nature Mater.*, 2011, **10**, 968-973.
13. X. Li, D. Shen, J. Yang, C. Yao, R. Che, F. Zhang and D. Zhao, *Chem. Mater.*, 2013, **25**, 106-112.
14. H. Wen, H. Zhu, X. Chen, T. F. Hung, B. Wang, G. Zhu, S. F. Yu and F. Wang, *Angew. Chem., Int. Ed.*, 2013, **52**, 13419-13423.
15. L. Liu, S. Wang, B. Zhao, P. Pei, Y. Fan, X. Li and F. Zhang, *Angew. Chem., Int. Ed.*, 2018, **57**, 7518-7522.
16. J. Zuo, D. Sun, L. Tu, Y. Wu, Y. Cao, B. Xue, Y. Zhang, Y. Chang, X. Liu, X. Kong, W. J. Buma, E. J. Meijer and H. Zhang, *Angew. Chem., Int. Ed.*, 2018, **57**, 3054-3058.
17. J. Zuo, L. Tu, Q. Li, Y. Feng, I. Que, Y. Zhang, X. Liu, B. Xue, L. J. Cruz, Y. Chang, H. Zhang and X. Kong, *ACS Nano*, 2018, **12**, 3217-3225.
18. H. Dong, L.-D. Sun, W. Feng, Y. Gu, F. Li and C.-H. Yan, *ACS Nano*, 2017, **11**, 3289-3297.
19. B. Chen, D. Peng, X. Chen, X. Qiao, X. Fan and F. Wang, *Angew. Chem., Int. Ed.*, 2015, **54**, 12788-12790.
20. C. Dong and F. C. J. M. van Veggel, *ACS Nano*, 2009, **3**, 123-130.
21. S. Dühnen and M. Haase, *Chem. Mater.*, 2015, **27**, 8375-8386.
22. D. Hudry, D. Busko, R. Popescu, D. Gerthsen, A. M. M. Abeykoon, C. Kübel, T. Bergfeldt and B. S. Richards, *Chem. Mater.*, 2017, **29**, 9238-9246.
23. D. H. Son, S. M. Hughes, Y. Yin and A. Paul Alivisatos, *Science*, 2004, **306**, 1009.
24. J. H. Chang, D. Hahm, K. Char and W. K. Bae, *Journal of Information Display*, 2017, **18**, 57-65.
25. L. De Trizio and L. Manna, *Chem. Rev.*, 2016, **116**, 10852-10887.
26. L. Zhou, Y. Fan, R. Wang, X. Li, L. Fan and F. Zhang, *Angew. Chem., Int. Ed.*, 2018, **57**, 12824-12829.
27. Y. Fan, P. Wang, Y. Lu, R. Wang, L. Zhou, X. Zheng, X. Li, J. A. Piper and F. Zhang, *Nature Nanotech.*, 2018.
28. G.-S. Yi and G.-M. Chow, *Chem. Mater.*, 2007, **19**, 341-343.
29. H.-S. Qian and Y. Zhang, *Langmuir*, 2008, **24**, 12123-12125.
30. N. J. J. Johnson, A. Korinek, C. Dong and F. C. J. M. van Veggel, *J. Am. Chem. Soc.*, 2012, **134**, 11068-11071.
31. C. Kind, R. Popescu, R. Schneider, E. Muller, D. Gerthsen and C. Feldmann, *RSC Adv.*, 2012, **2**, 9473-9487.
32. D. Hudry, A. M. M. Abeykoon, E. Dooryhee, D. Nykypanchuk and J. H. Dickerson, *Chem. Mater.*, 2016, **28**, 8752-8763.

33. R. Shannon, *Acta Cryst.*, 1976, **32**, 751-767.
34. S. Wen, J. Zhou, K. Zheng, A. Bednarkiewicz, X. Liu and D. Jin, *Nature Communications*, 2018, **9**, 2415.

Interface Disorder in Large Single- and Multi-Shell Upconverting Nanocrystals.

Damien Hudry,[1] Radian Popescu,[2] Dmitry Busko,[1] Maria Diaz-Lopez,[3] Milinda Abeykoon,[4] Pierre Bordet,[3] Dagmar Gerthsen,[2] Ian A. Howard,[1, 5] and Bryce S. Richards*[1,5]*

[1] Institute of Microstructure Technology, Karlsruhe Institute of Technology, Hermann-von-Helmholtz-Platz 1, D-76344 Eggenstein-Leopoldshafen, Germany.

[2] Laboratory of Electron Microscopy, Karlsruhe Institute of Technology, Engesserstrasse 7, D-76131 Karlsruhe, Germany.

[3] Université Grenoble Alpes, CNRS, Institut Néel, 38000 Grenoble, France.

[4] Photon Science Division, National Synchrotron Light Source II, Brookhaven National Laboratory, Upton, New York 11973, United States.

[5] Light Technology Institute, Karlsruhe Institute of Technology, Engesserstrasse 13, D-76131 Karlsruhe, Germany.

Table of Contents

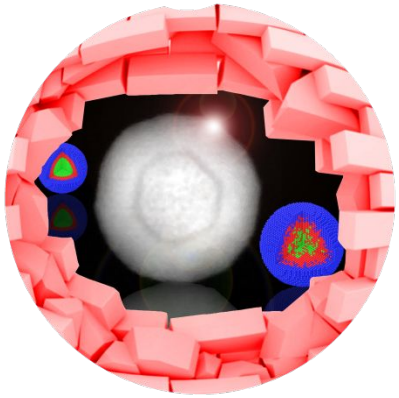

Behind-the-shells. Single- and multi-shell upconverting nanocrystals, with their increasing numbers of applications, are characterized by core-shell and shell-shell interfaces, which are not yet fully understood. In this contribution, the magnitude of interface disorder in large single- and multi-shell nanocrystals is investigated. It sheds new light on the chemical and structural organization of such complex functional materials that should be described as non-periodic modulated structures over a large size regime.